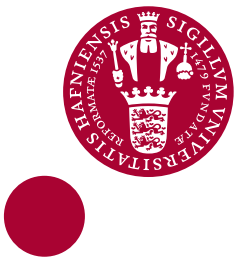

Mechano-signalling, induced by fullerene C60 nanofilms, arrests the cell cycle in the G2/M phase and decreases proliferation of liver cancer cells

Sosnowska, Malwina Ewa; Kutwin, Marta; Jaworski, Slawomir; Strojny, Barbara; Wierzbicki, Mateusz; Szczepaniak, Jaroslaw; ojkowski, Maciej; wiszkowski, Wojciech; Baaban, Jamina; Chwalibog, André; Sawosz, Ewa

Published in:
International Journal of Nanomedicine

DOI:
10.2147/IJN.S206934

Publication date:
2019

Document version
Publisher's PDF, also known as Version of record

International Journal of Nanomedicine

Dovepress
open access to scientific and medical research

Open Access Full Text Article

ORIGINAL RESEARCH

Mechano-signalling, induced by fullerene C_{60} nanofilms, arrests the cell cycle in the G2/M phase and decreases proliferation of liver cancer cells

This article was published in the following Dove Press journal:
International Journal of Nanomedicine

Malwina Sosnowska[1]
Marta Kutwin[1]
Sławomir Jaworski[1]
Barbara Strojny[1]
Mateusz Wierzbicki[1]
Jarosław Szczepaniak[1]
Maciej Łojkowski[2]
Wojciech Święszkowski[2]
Jaśmina Bałaban[1]
André Chwalibog[3]
Ewa Sawosz[1]

[1]Department of Animal Nutrition and Biotechnology, Warsaw University of Life Sciences, Warsaw 02-786, Poland; [2]Faculty of Materials Science and Engineering, Warsaw University of Technology, Warsaw 00-661, Poland; [3]Department of Veterinary and Animal Sciences, University of Copenhagen, Frederiksberg 1870, Denmark

Introduction and objective: Degradation of the extracellular matrix (ECM) changes the physicochemical properties and dysregulates ECM–cell interactions, leading to several pathological conditions, such as invasive cancer. Carbon nanofilm, as a biocompatible and easy to functionalize material, could be used to mimic ECM structures, changing cancer cell behavior to perform like normal cells.

Methods: Experiments were performed in vitro with HS-5 cells (as a control) and HepG2 and C3A cancer cells. An aqueous solution of fullerene C_{60} was used to form a nanofilm. The morphological properties of cells cultivated on C_{60} nanofilms were evaluated with light, confocal, electron and atomic force microscopy. The cell viability and proliferation were measured by XTT and BrdU assays. Immunoblotting and flow cytometry were used to evaluate the expression level of proliferating cell nuclear antigen and determine the number of cells in the G2/M phase.

Results: All cell lines were spread on C_{60} nanofilms, showing a high affinity to the nanofilm surface. We found that C_{60} nanofilm mimicked the niche/ECM of cells, was biocompatible and non-toxic, but the mechanical signal from C_{60} nanofilm created an environment that affected the cell cycle and reduced cell proliferation.

Conclusion: The results indicate that C_{60} nanofilms might be a suitable, substitute component for the niche of cancer cells. The incorporation of fullerene C_{60} in the ECM/niche may be an alternative treatment for hepatocellular carcinoma.

Keywords: liver cancer cells, fullerene, extracellular matrix, adhesion, cell cycle

Introduction

Hepatocellular carcinoma (HCC) is the third most common cause of cancer-related mortality and the fifth most common malignancy worldwide.[1,2] The poor prognosis of HCC is mainly due to the development of distant metastasis.[3] Furthermore, people with fibrosis and cirrhosis of the liver, resulting from viral factors and alcohol intake, belong to the group at risk for HCC.[2,4,5] According to some research, the extracellular matrix (ECM) composition of liver fibrosis is connected to changes in matrix stiffness, flexibility and density, because of the dysregulation of predominant collagen, elastic fibers and other structural features.[6]

The elastic modulus of mammalian cells ranges between 1 and 100 kPa. The elastic modulus is different between cell types and identifies diseased cells, particularly, cancer cells.[7,8] Generally, cancerous cells (MCF-7, T47D, PC-3, Du145 and LNCaP) are softer and easier to deform than benign cells (MCF-10A) due to

Correspondence: André Chwalibog
Department of Veterinary and Animal Sciences, University of Copenhagen, Groennegaardsvej 3, Frederiksberg 1870, Denmark
Tel +45 4 096 3573
Email ach@sund.ku.dk

http://doi.org/10.2147/IJN.S206934

reduction in the F-actin or/and stress fibers.[9,10] Moreover, some studies on breast cancer indicate a correlation between tissue elasticity and cancer malignancy,[11] and furthermore, the tumor initiation, progression and metastasis were observed under the influence of collagen stiffness.[12] Recent studies indicated that the biomechanical environment, in particular ECM stiffness, modulates cell behavior and phenotype.[13] Schrader et al reported that a niche with high stiffness fosters HCC cellular proliferation, but a soft niche induces cellular dormancy.[1] Extracellular components play an important role during cancer progression. Niche remodeling and growth in abnormal microenvironments lead to tumor-like cell behavior.[14] Undoubtedly, the reconstruction of the ECM/niche, and especially its mechanical properties, may restore a normal phenotype in cancer cells.[8]

Cell contact with the ECM/niche converts mechanical stimuli into a chemical signal. The first recognition of physical stimulation occurs via the intracellular domain of integrins that connect to the cytoskeleton.[15] Integrins are involved in migration and anchor invasive cancer cells to the ECM.[16] Anchoring cells to a niche allows the cell polarity to be maintained and asymmetric cell division to occur, which determines the cell's fate.[17] Thus, the behavior of cancer cells can be modified, particularly, the inhibition of overproliferation.[18,19] The activities of multiple cell-polarity and cell-adhesion genes, which are regulated by non-canonical 3-D tissue polarity, may lead to tumor suppression.[20] Nevertheless, the 3-D structure of tissue requires the unique composition and topography of ECM components as well as ECM dynamics by active metalloproteinases.[18]

The contact of cells with microenvironment leads to the recruitment of integrins as well as various proteins to the plasma membrane, such as focal adhesion kinase, talin, vinculin, paxillin and actopaxin. Other adhesion proteins, such as cadherins, are also sensitive to mechanical load and their composition and expression depend on the cell environment.[21] More than 125 structural and regulatory proteins are involved in the formation of so-called focal adhesions (FAs).[15,22] The mechanical connection between FAs, the cytoskeleton and the nucleus allows transduction of the signal to the lamin A/C of the nuclear membrane. Local strength can generate flattening of the nucleus, the dynamics of chromatin and pores and regulate gene transcription, which leads to increased nuclear import.[23,24]

Cells can detect ECM rigidity and roughness that matches the cells' intrinsic elasticity.[25] A local increase in ECM rigidity in soft tissues leads to increased proliferation and migration due to the generation of large cellular forces, formation of focal adhesions and abundant stress fibers.[26] As mentioned previously, Schrader et al reported that a soft niche induces cellular dormancy.[1] The mechanism of this process, however, is not entirely clear. Wong et al reported that cells use filopodia extensions to probe substrate rigidity.[27] The lamellipodia and filopodia play a major role in driving cell migration by attaching cells to the niche.[28] However, some niches can change cell morphology. During migration, the cell needs to degrade and remodulate its environment using invadopodia.[29] The type IV collagen network, containing pores on the order of 100 nm, is regarded as the physical barrier to cells. Thus, degradation and reduction of basement membrane synthesis may contribute to metastasis.[13] Therefore, it seems that the interaction between the cell and its niche is subjected to a mutual active modulation and determines cell behavior.

Taking the above into consideration, it appears that a modification of the ECM/niche or the application of an ECM/niche equivalent is necessary to reduce the proliferation of cancer cells. The perfect niche should be non-toxic and have optimal physicochemical properties, specifically, elasticity, porosity and the presence of specific chemical groups on the surface.[30] Carbon nanomaterials, especially fullerenes, could be promising materials because of their moderate toxicity. Fullerenes may play a role as an effective platform for drug delivery,[31] in particular, pristine fullerene C_{60} modulates oxidative stress, inhibits angiogenesis and shows non-toxic activity at low concentrations.[32,33] Furthermore, C_{60} significantly reduces the negative aspect of chemotherapeutics and can enhance their anti-cancer activity.[33–36] Although toxic effects of fullerenes were also observed, the form of administration influenced the level of toxicity.[37,38] Some research groups have shown that C_{60} has no acute toxicity in vitro[39] or in vivo[40] and that the level of toxicity is related to the cell type.[41]

Most often, C_{60} is administered to the medium and results are based on the uptake of C_{60} by the cell and its nucleus.[42] Raoof et al provided evidence for the internalization of derivatives C_{60}-serPF and C_{70}-gallic acid within living Hep3B and HT-29 cells and accumulation in the subcellular organelles, such as nuclei and lysosomes.[43,44] The nucleus is the intended target for cancer therapy due to inhibition of uncontrolled proliferation by uptake of C_{60}. This uptake is dependent on cell lines but independent of the phase of the cell cycle. Because of the small size, C_{60} permeates into nucleus via passive diffusion, direct penetration or

endocytosis, then forming aggregates in association with chromatin. However, in the present study, we assumed that C_{60} used as a surface would mechanically affect cells but could not be internalized by cells. Consequently, C_{60} may be a surface component that improves the mechanical features of the ECM. In the present study, we hypothesized that C_{60} nanofilm can influence the expression of α5β1 integrin, N-cadherin, β-catenin, vinculin, alter the cytoskeleton structure and inhibit proliferation via the mechanotransduction mechanism. The objective of our study was to use carbon nanostructures as an artificial ECM-like structure that should be perceived by cancer cells as a friendly, pro-adhesive material, while simultaneously acting as a source of mechanotransduction signaling, which would modify cancer cell behavior via the adhesion proteins-dependent mechanism, consequently leading to reduced cell proliferation.

Materials and methods

Preparation and characterization of fullerenes (C_{60}) and nanofilms (C_{60})

Characterization of C_{60} nanoparticles

Fullerenes (C_{60}) nanoparticles were purchased as a powder from SES Research (Houston, TX, USA) and produced by the arc discharge method. This nanomaterial, after dispersion into ultrapure Milli-Q water to prepare 50 mg/L solutions, was sonicated for 15 mins in an ultrasonic bath (Bandelin Electronic, Berlin, Germany) to avoid agglomeration. The shape and size of the C_{60} nanoparticles were characterized using transmission electron microscopy (TEM: JEM-1220 JEOL, Tokyo, Japan) and the zeta potential was measured with a Nano-ZS90 Zetasizer (Malvern Instruments, Malvern, UK), according to the procedures described by Sawosz et al.[45]

Characterization of C_{60} nanofilms

A C_{60} aqueous solution was used to form nanofilm by applying the solution to the bottom of the wells in 6-well plates and allowing them to dry. The resultant surface, as a result of self-assembly, was a stable, thin surface nanofilm that adhered perfectly to the bottom of the plastic wells.

To determine the functional groups of C_{60}, the Fourier transform infrared (FTIR) spectra were registered using a Nicolet 8700 FT-IR spectrometer (Thermo Scientific, Waltham, MA, USA) in the range of 4000–400 cm^{-1}. Solid-state samples were milled with potassium bromide crystals at an approximate ratio of 1:200 mg. A total of 100 scans were completed per sample. The infrared absorption of water vapor and carbon dioxide was mostly eliminated. Spectra were presented as transmittance (dependent variable) against wavenumber (independent variable).

Atomic force microscopy (AFM) was used for the characterization of the C_{60} surface morphology. The C_{60} nanofilm has been deposited from the solution on the cell culture plates in the form of droplets which evaporated and the thin films of C_{60} on the plates were obtained. Then, the AFM was performed directly on the coated and uncoated plates in liquid environment. The AFM imaging was performed in the conditions as similar to the environment found during cell culture as possible. AFM imaging was performed using the MFP 3D Bio AFM with a commercial triangular cantilever (MLCT Bruker, Camarillo, CA, USA), with a spring constant of k =0.10 N/m, in AC mode, in air.

To evaluate the affinity of cells to the nanofilm, 10 µL droplets of the C_{60} colloidal solution, at a concentration of 1000 mg/L, were embedded at the surface of the wells in 6-well plates according to the pattern of dots (Figure 1A).[46] After dried nanofilm dots were present at the bottom of 6-well plates, we were able to observe the preferences of cell placement on and outside the nanofilm.

Cell cultures

Liver cancer cell lines, HepG2 (HB-8065) and C3A (CRL-10741), and a non-cancer bone marrow stromal cell line, HS-5 (CRL-11882), were obtained from the American Type Culture Collection (ATCC, Manassas, VA, USA). The cell cultures were maintained at 37°C, under 5% CO_2, in Dulbecco's Modified Eagle Medium, Low Glucose (DMEM, Gibco, Thermo Scientific, Waltham, MA, USA), supplemented with 10% foetal bovine serum (FBS, Life Technologies, Houston, TX, USA), penicillin (100 U/mL) and streptomycin (100 mg/mL, Life Technologies, Grand Island, NY, USA). Cells were seeded on 6-well plates (1.5×10^5 HS-5 cells, 2.0×10^5 HepG2 and C3A cells in each well), with the preformed nanofilm patterns or without nanofilms, as a control. The cultures were maintained for 7 days without medium changes.

Cell viability and proliferation

XTT assay

Viability assessment of cancer cells (HepG2 and C3A) and control cells (HS-5), seeded on the C_{60} nanofilms, was performed using the XTT test (Roche Protocol, Mannheim, Germany). The solution of nanoparticles (20 µg) was dropped on the bottom of wells of 96-well microplates and dried. Cells were then seeded on the 96-well microplates with

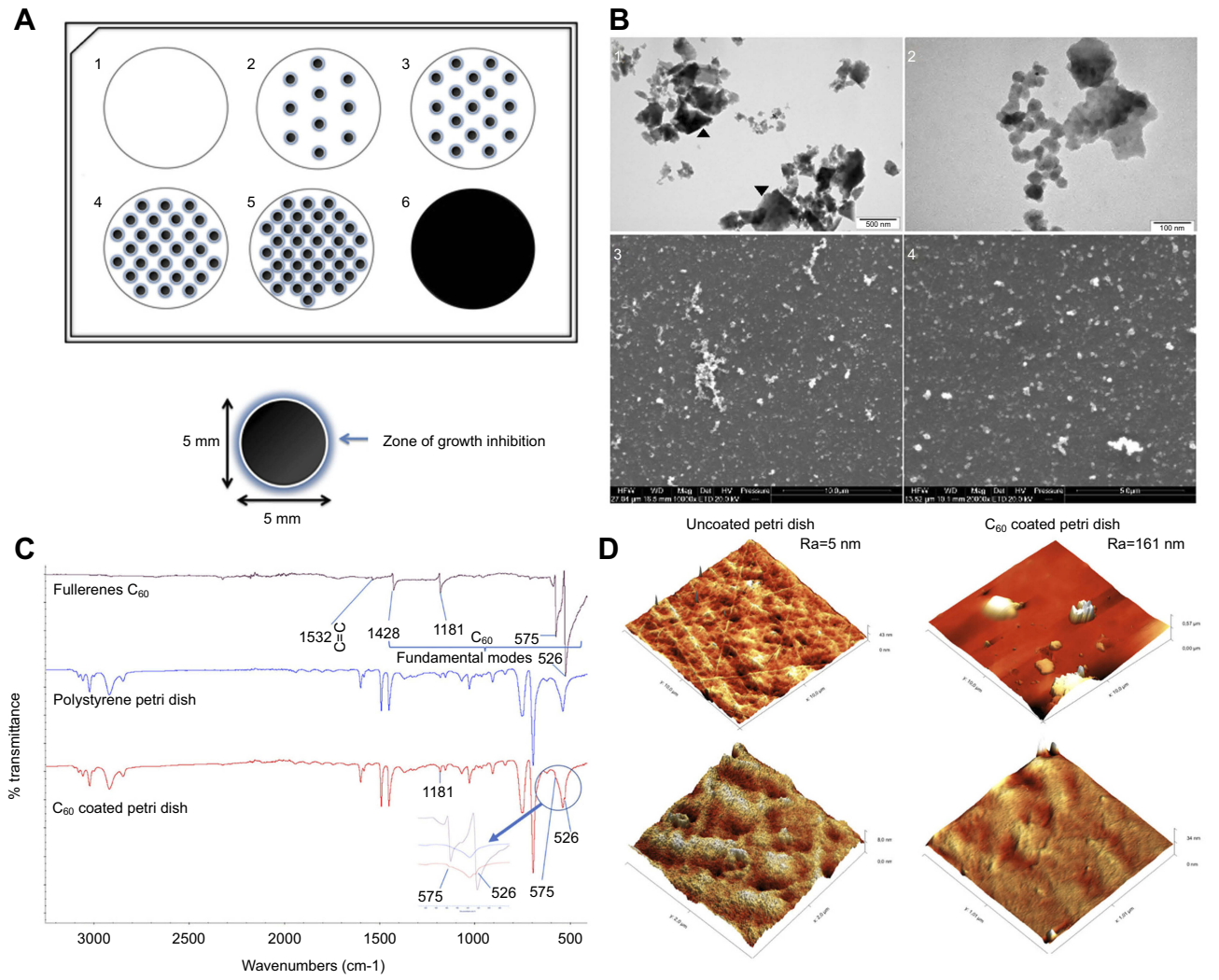

Figure 1 Preparation and characterization of C_{60} nanofilms.

Notes: (**A**) Nanofilms pattern of dots: 1=0 dots (control); 2=10 dots, C_{60}-20%; 3=17 dots; 4=28 dots; 5=37 dots; 6= covering the entire surface, C_{60}-100%. (**B**) Characterization of fullerenes by transmission electron microscopy (TEM) (1, 2) and scanning electron microscopy (SEM) (3, 4). Scale bars: 500 nm (1), 100 nm (2), 10 μm (3) and 5 μm (4). Agglomerates were observed in the colloid of nanoparticles (black arrowheads). (**C**) Infrared spectrum of C_{60} registered in the middle region (3500–500 cm^{-1}). Characteristic transmission bands were assigned to the appropriate vibrations of groups and bands present in the studied samples. (**D**) Comparison between the Petri dish uncoated and coated with C_{60} made by means of AFM. The side width of the images is 10 μm for the upper row and 2 μm for the lower. The left micrographs are of the uncoated plate and the right micrographs are of the C_{60} coated plate.

Abbreviations: C_{60}, fullerenes; Ra, roughness (nm).

nanofilms (or without as a control) in a volume of 100 μL, at a concentration of 8×10^3 (HS-5) and 1×10^4 (HepG2, C3A) cells per well. After 24 hrs, the XTT solution (50 μL) was added to each well and incubated for 1 hr at 37°C. Results were examined using a Tecan Infinite 200 microplate reader (Tecan, Durham, NC, USA) according to the manufacturer's instructions. Cell viability was expressed as the percentage of $(OD_{test} - OD_{blank})/(OD_{control} - OD_{blank})$, where OD_{test} is the optical density of cells seeded on nanofilms, $OD_{control}$ is the optical density of the control sample (cells seeded in wells without nanofilms) and OD_{blank} is the optical density of wells without cells but with nanofilms.

Trypan blue assay

HS-5, HepG2 and C3A cells were cultivated as described in the section "Cell cultures". After a week, the cell cultures were washed in PBS and dissociated by using 0.25% trypsin and neutralized in fresh DMEM medium. The total cell count and live cell count were evaluated by using trypan blue (NanoEnTek, Waltham, MA, USA). A mixture of the cell suspension (10 μL) and 0.4% trypan blue solution (10 μL) was prepared. Next, an aliquot (10 μL) of the mixture was placed onto cell counting slides and counted by the EVE™ automatic cell counter (NanoEnTek, Waltham, MA, USA). The percentage of

the live cells cultivated on C_{60} was expressed as the live cells count compared to the control.

BrdU assay

Cell proliferation was studied using a bromodeoxyuridine (BrdU) incorporation assay (BrdU colorimetric) (Roche Applied Science, Indianapolis, IN, USA). The solution of C_{60} nanoparticles was dropped (20 µg) on the bottom of the wells of 96-well microplates and dried. HS-5, HepG2 and C3A cells were seeded on the 96-well microplates with C_{60} nanofilms or without (control) at a concentration 8×10^3 cells. Cells were cultivated for 48 hrs and then 20 µL of 100 µM BrdU solution, in DMEM, was added to each well of the cultured cells. The cells were labeled with BrdU for 24 hrs. All further steps were carried out according to the manufacturer. Cell proliferation was analyzed by a Tecan Infinite 200 microplate reader (Tecan, Durham, NC, USA) at 370 nm with a reference wavelength of 492 nm.

Microscopy

Light microscopy

To assess the morphology of cells grown on the C_{60} surface, C_{60} dots and blank wells (control wells) of 6-well plates were examined using an inverted light microscope (Leica, TL-LED, Wetzlar, Germany), connected to a digital camera (Leica MC190 HD), using LAS V4.10 software (Leica, Wetzlar, Germany). The cells were stained using hematoxylin-eosin (H+E).

SEM microscopy

Details of cell morphology were evaluated using scanning electron microscopy (SEM: Zeiss, Ultra Plus, Oberkochen, Germany). HS-5, HepG2 and C3A cells were seeded on 6-well plates coated with nanofilm of C_{60} dots. SEM observations of cells were completed with a Quanta 200 electron microscope (FEI, Hillsboro, OR, USA). Cells were prepared for SEM observation after 7 days of exposure to the C_{60} nanofilms. The cells were rinsed in phosphate-buffered saline (PBS, pH 7.2), then fixed in 2.5% glutaraldehyde (G5882, Sigma-Aldrich, St. Louis, MO, USA) for 30 mins. Cells were contrasted and dehydrated according to Wierzbicki et al.[47] Samples were placed on aluminum SEM stubs. Subsequently, cells were dehydrated in increasing concentrations of hexylene glycol (Sigma-Aldrich, St. Louis, MO, USA). Drying was performed with a Polaron CPD 7501 critical point dryer (Quorum Technologies, Laughton, UK).

Confocal microscopy

Confocal microscopy was used to evaluate integrin α5β1 expression and F-actin filaments and nuclei topography. Cells were seeded on 6-well plates, as described in the section "Cell cultures", containing coverslips with nine dots of C_{60} nanofilms. After a week, cells were washed three times in PBS without Ca^+ and Mg^{2+} and fixed with 4% paraformaldehyde (Sigma, St. Louis, MO, USA) in phosphate buffer (0.1 M, pH 7.2) for 10 mins. After fixation, the coverslips with cells were washed and permeabilized with 0.5% Tween 20 (Sigma, St. Louis, MO, USA) PBS solution for 10 mins. Further, non-specific binding was blocked by incubating the cells with PBS containing 2% goat serum, 1% bovine serum albumin (Sigma, St. Louis, MO, USA) and 0.25% glycine for 30 mins. The mouse monoclonal antibody, anti-integrin α5β1 (clone JBS5, Merck Millipore, Billerica, MA, USA), was diluted to 1:200 in 1% bovine serum albumin, and then cells were incubated at 4°C overnight with the antibody. The secondary antibody for anti-integrin α5β1, goat anti-mouse FITC 488 conjugate (Sigma, St. Louis, USA), was diluted to 1:100 and incubated with the cells for 2 hrs. Cell nuclei and F-actin filaments were stained with 4′,6-diamidino-2-phenylindole (DAPI, Thermo Fisher Scientific, Waltham, MA, USA) and phalloidin-Atto 633 (Sigma, St. Louis, MO, USA), respectively. The cells were observed under 60× magnification using an inverted confocal microscope, IX 81 FV-1000 (Olympus Corporation, Tokyo, Japan).

Atomic force microscopy

Force spectroscopy was used to investigate the change of the elastic moduli of cells cultivated on C_{60} nanofilms in comparison to the control cell culture (not cultivated on nanofilms). Force spectroscopy was performed on the MFP 3DBio AFM. AFM, operated in the force spectroscopy mode, allowed the acquisition of elastic moduli maps of single cells. In the case of the single cell imaging, maps 50 µm × 50 µm large, consisting of 44 × 44 points, where each of these points represented a force–distance curve, were gathered. Each force–distance curve contained information about the displacement of the cell membrane in response to the applied force. Elastic moduli can be computed from the analysis of the force curve.[48] Cells were indented with the RC800PSA cantilever (Olympus Corporation, Tokyo, Japan), with a spring constant of k=0.05 N/m and the following dimensions: 200 µm × 20 µm. Implemented with AFM Asylum Research software was used to calibrate the

cantilever before each experiment. It is widely accepted to use the Hertz model for force–distance curve analysis.[49] Cells from each cell line were measured. The mean value of the elastic moduli was calculated for each cell. No suitable measurements were rejected.

Immunoblotting

Immunoblotting methods were used to evaluate β-catenin, N-cadherin, vinculin and proliferating cell nuclear antigen (PCNA). The cells were cultured as described in the section "Cell cultures", and they were then scraped and centrifuged at 1200 rpm for 10 mins. Whole-cell protein extracts were prepared using an ice-cold radioimmunoprecipitation assay (RIPA), supplemented with protease and phosphatase inhibitors (Sigma-Aldrich, St. Louis, MO, USA) at a ratio of 100:1 (RIPA: protease and phosphatase inhibitors). After centrifugation for 30 mins at 12,000× g at 4°C, the supernatant containing the protein extracts was removed. The protein concentration was measured using a Bicinchoninic Acid Kit (Sigma-Aldrich, St. Louis, MO, USA). Sample buffer containing β-mercaptoethanol (Bio-Rad Laboratories, Munich, Germany) was added and the proteins were denatured for 5 mins. Equal amounts of protein from each sample were loaded onto a 10% polyacrylamide gel. Electrophoresis was run at 100 mA, 100 V, for 2 hrs in 25 mm Tris-glycine-sodium dodecyl sulfate (SDS) buffer. After electrophoresis, proteins were transferred to polyvinylidene difluoride (PVDF) membranes with a Trans-Blot Turbo Transfer System (Bio-Rad Laboratories, Munich, Germany). Membranes were blocked with 5% non-fat milk (Bio-Rad Laboratories, Munich, Germany) in PBS for 60 mins. Membranes were then incubated with the primary antibody: β-catenin polyclonal antibody (No. PA5-19469, Thermo Fisher Scientific, Waltham, MA, USA), N-cadherin monoclonal antibody (No. MA1-159, Thermo Fisher Scientific, Waltham, MA, USA), vinculin monoclonal antibody (No. 700062, Thermo Fisher Scientific, Waltham, MA, USA) and PCNA monoclonal antibody (No. 13–3900, Life Technologies Rockford, IL, USA). After overnight incubation at 4°C, membranes were washed in PBS and incubated with the diluted secondary antibody, goat anti-mouse IgG, IgM (H+L) (No. T2192, Applied Biosystems, Bedford, MA, USA) or goat anti-rabbit IgG (H+L) (No. T1048, Applied Biosystems, Bedford, MA, USA) for 1 hr. For immunodetection of the proteins, the Western-Star™ Immunodetection System (No. T1046, Applied Biosystems) was used. Stripping of primary and secondary antibodies from blots was performed using Restore Western Blot Stripping Buffer (No. 21059, Thermo Scientific). Glyceraldehyde-3-phosphate dehydrogenase (GAPDH, MA5-15738, Thermo Fisher Scientific, Waltham, MA, USA) was used as a loading control for protein normalization. The protein expression was visualized using Azure c400 (Azure Biosystems, Dublin, CA, USA) and background corrections were carried out with ImageJ® 1.48v (National Institutes of Health, Bethesda, MD, USA).

Flow cytometry

The cell cycle was evaluated using flow cytometry. Cells were cultured in 6-well plates for a week, as described in the section "Cell cultures". The medium was removed, and cells were detached with trypsin. The trypsin was neutralized with fresh DMEM medium. The mixture was centrifuged at 1200 rpm for 10 mins. Cell-cycle analysis, based on DNA content, was performed according to the UC San Diego Health Sciences protocol.[50] The protocol consisted of two steps: 1) fixation of cells and 2) staining with propidium iodide (PI, 500 µg/mL). The cells were washed twice with PBS, resuspended in PBS (1 mL) and fixed with 9 volumes of 70% ethanol at 4°C for 24 hrs. After centrifugation, each sample of cells was resuspended in 500 µL of staining solution. The staining solution contained RNAse A (2 µL, Thermo Fisher Scientific, Waltham, MA, USA), PI (20 µL, Thermo Fisher Scientific, Waltham, MA, USA), Tween 20 (0.5 µL) and PBS (477.5 µL). After incubating for 30 mins, cells were analyzed by flow cytometry (FACSCalibur, Becton Dickinson, Franklin Lakes, NJ, USA), measuring the fluorescence emission at 530 nm and 575 nm (or equivalent), using excitation at 488 nm.

Statistical analysis

The data were analyzed using one-way analysis of variance (ANOVA) with Tukey's post-hoc test by using Statgraphics Plus 4.1 (StatPoint Technologies, Warrenton, VA, USA). Differences at with a P-value ≤0.05 were defined as statistically significant.

Results

Characterization of C_{60} and C_{60} nanofilm

Fullerenes (C_{60}) nanoparticles were polyhedron-shaped and were 15–50 nm in size (Figures 1B2 and B4). After drying, C_{60} showed a tendency to agglomerate (Figures 1B1 and B3). The zeta potential of the hydrocolloid was −30.5 mV.

Figure 1C presents the FTIR spectra of C_{60} fullerenes, the polystyrene culture plate and the plate covered with a thin film of the fullerenes. Bands identified and assigned in the IR spectrum were typical to spectra of C_{60} measured by

Saeedfar et al.[51] The spectrum for fullerenes contains several bands throughout the entire spectral region registered. A weak peak in the C_{60} fullerenes spectrum, at 1532 cm^{-1}, is a sign of a carbon–carbon double bond stretching vibrations. The remaining bands, occurring in whole spectral regions, were the fundamental modes characteristic of C_{60} at 1428, 1181, 575 and 526 cm^{-1}. The spectrum of the plate was a typical spectrum of polystyrene as compared with the reference spectrum of polystyrene in the reference library of polymer spectra. The spectrum of the plate coated with the fullerenes thin film was slightly modified in comparison to uncoated plate. However, the signal from the polystyrene strongly overlapped with the fullerene spectra. The peak in the plate spectra coated with the nanofilm in the range of 500–600 cm^{-1} was slightly modified in comparison to the spectra of the uncoated plate. Overlying peaks from C_{60} fullerene were seen at 575 and 526 cm^{-1}. Also, the intensity of the peak at 1181 cm^{-1} was slightly increased in comparison to the spectra of the uncoated plate.

The AFM provided information about the topography of the investigated samples. Figure 1D shows the AFM micrographs of the plate with and without C_{60} film. The average roughness of the uncoated surface was Ra=5 nm, while the roughness of the C_{60} coated surface was Ra=161 nm, for 10 μm × 10 μm images. The images with higher magnification (side width of the image: 2 μm) showed that the texture of the coated plates become blurred due to the C_{60} nanofilm has filled all the groves in the plate.

Evaluation of biocompatibility of C_{60} nanofilm

The influence of the C_{60} nanofilms on the viability of HS-5, HepG2 and C3A cells was examined using the XTT test (Figure 2B). The C_{60} nanofilm significantly reduced the viability of the HS-5 cell line by 37% (p=0.0054). The C_{60} nanofilm did not reduce the survival of cancer cells, as viability changes were insignificant. These results allowed us to demonstrate the biocompatibility of C_{60} nanofilms and use it as an ECM equivalent for cell cultivation in the following experiments.

After a week of culturing, single dead cells were observed, which was statistically insignificant (Figure S1). To determine whether carbon nanofilms influenced the cell viability, especially when cells have a free choice of location and may migrate and settle on a nanofilm according to their preference, experiments with nanofilm dots were performed. The effect of the preferential settlement on the different nanofilms in relation to cell number was evaluated. Covering the surface with C_{60} at 100% reduced the total number of all cells. The C_{60} nanofilm dots favored the settlement of C3A cells but reduced the number of HepG2 cells and slightly decreased the population of HS-5 cells.

Cell proliferation was measured with the BrdU test (Figure 2C). During the BrdU assay, the thymidine analog, BrdU, was incorporated into replicating cellular DNA and was detected using anti-BrdU antibodies. C_{60} nanofilms reduced the proliferation of HS-5 cells by more than 20% (p=0.0120) compared to the control group. However, a small, but statistically insignificant decrease was observed for HepG2 cells growing on C_{60} nanofilms. Furthermore, C_{60} nanofilms caused a slight increase in the proliferation of C3A cells.

To confirm the effect of C_{60} nanofilms on cell proliferation, PCNA was examined (Figure 3E). The expression level of PCNA was reduced in HS-5 and HepG2 cells cultured on C_{60} nanofilms, where the greatest reduction in proliferation was observed in HepG2 cells. However, PCNA protein expression increased in C3A cells on C_{60}.

Influence of C_{60} nanofilm on cell morphology

Cell morphology was visualized using light microscopy and SEM. Nanofilms, placed as dots, allowed us to observe the cell morphology on nanofilm dots, outside dots, and on the border of the dots (Figures 4–6). The cells cultivated without nanofilms (control) had characteristic morphologies for their cell type. In general, C_{60} nanofilms did not induce drastic morphological changes of the cells.

However, all cell lines showed changes in polarization and shape, depending on the location, in relation to the biofilm dot. Based on a study by Chen et al,[52] we determined the direction of migration of individual cells. The cells were spread on nanofilms and migrated along the long axis and extended lamellipodium. The individual liver cells avoided contact with the nanofilm, but in the clusters, were preferentially located on the border of C_{60} nanofilm dot.

The HepG2 and C3A cell clusters, unlike single HS-5 cells, were placed closely to the C_{60} nanofilm, especially to the dot border. The formation of cell clusters is characteristic of epithelial cells, ie, HepG2 and C3A. However, cell growth on the C_{60} nanofilm resulted in decreased intercellular connections in clusters and increased cell-cell distance compared to the control.

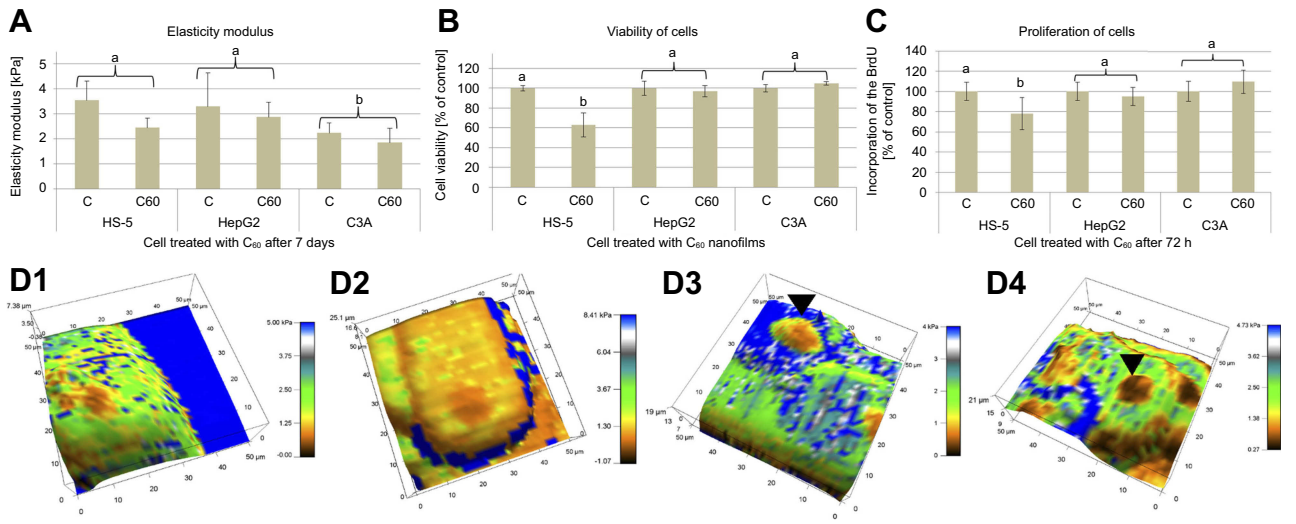

Figure 2 (**A**) Elasticity modulus (kPa) of HS-5, HepG2 and C3A cells on C_{60} nanofilms. (**B**) Viability of HS-5, HepG2 and C3A cells after growth on 20 μg of C_{60} nanofilms. (**C**) Proliferation of HS-5, HepG2 and C3A cells on C_{60} nanofilms. (**D**) Three-dimensional AFM images of HepG2 (**D1, D2**) and C3A (**D3, D4**) cells.

Notes: The differences between the cell lines were significant ($P \leq 0.05$). Different letters indicate significant differences between the groups (ANOVA, Tukey's post-test). The differences between the carbon-grown groups (20 μg of C_{60} nanofilm) and the control group were significant ($P \leq 0.05$) (ANOVA, Tukey's post-test) for HS-5 cells. Different letters indicate significant differences between the groups. Controls are shown in the pictures D1 and D3. The cell nuclei (black arrowheads) were observed using AFM.

Abbreviations: ANOVA, analysis of variance; C, control; C_{60}, fullerenes; XTT, 2,3-bis(2-methoxy-4-nitro-5-sulfophenyl)-5-[(phenylamino)carbonyl]-2H-tetrazolium hydroxide; BrdU, 5-bromo-2′-deoxyuridine. AFM, atomic force microscopy.

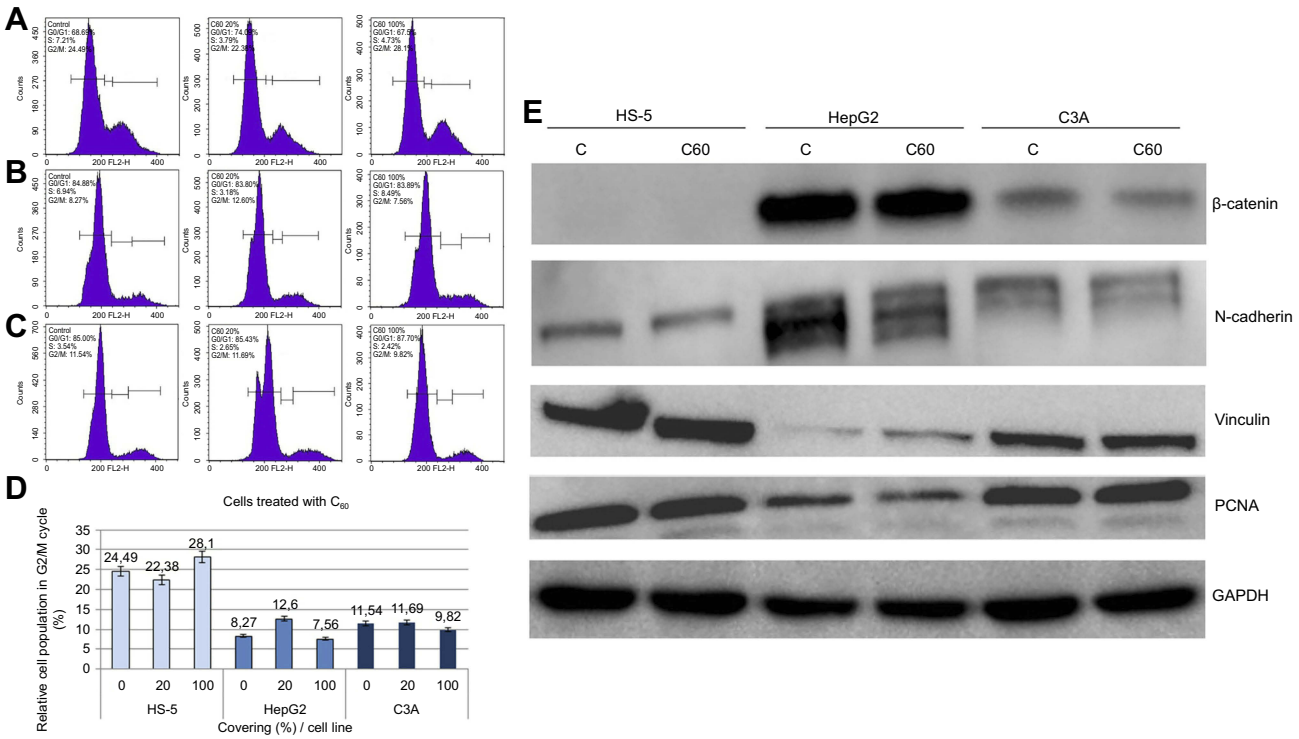

Figure 3 Propidium iodide (PI) 488 assay analysis.

Notes: Effect of C_{60} on the number (percentage) of (**A**) HS-5, (**B**) HepG2 or (**C**) C3A cells in the cycle phases. (**D**) Relative HS-5, HepG2 and C3A cell population in G2/M cycle (%). (**E**) Western blot analysis of β-catenin, N-cadherin, vinculin and PCNA. GAPDH was used as a loading control.

Abbreviations: C_{60}, fullerenes; GAPDH, glyceraldehyde 3-phosphate dehydrogenase; PCNA, proliferating cell nuclear antigen.

High magnification SEM images showed lamellipodia and filopodia of HS-5 cells (Figure 7A1 and A2). The cells were spread on C_{60} nanofilms and showed affinity to the nanofilm border by large lamellipodia and numerous, thin filopodia (Figure 7A2). The number of cells was comparable but slightly smaller on the nanofilm surface than outside dots (Figure 7A3).

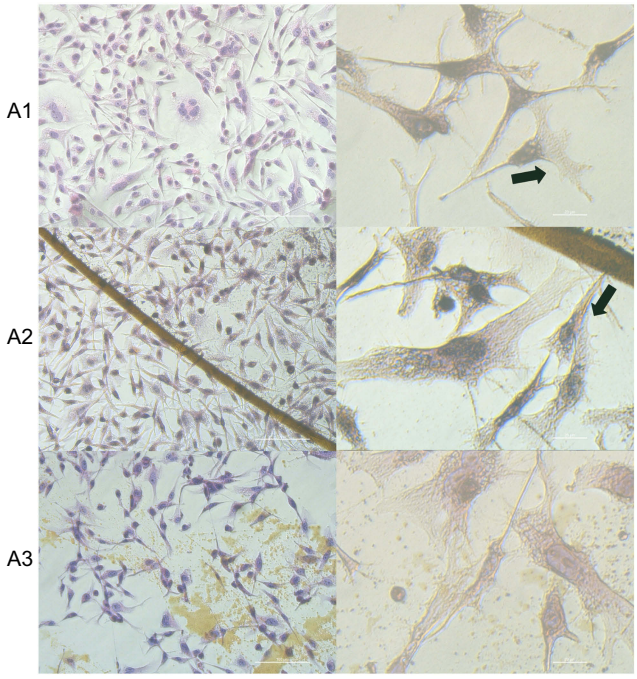

Figure 4 Morphology changes and affinity of HS-5 cells to the C_{60} nanofilms.
Notes: Hematoxylin-eosin (H+E) staining of HS-5 cells on C_{60} nanofilms visualized using light optical microscopy. (**A1**) control group; (**A2**) C_{60}-20%; and (**A3**): C_{60}-100%. Black arrows indicate the direction of cell migration. Scale bars: left pictures 100 μm; right pictures 20 μm.
Abbreviation: C_{60}, fullerenes.

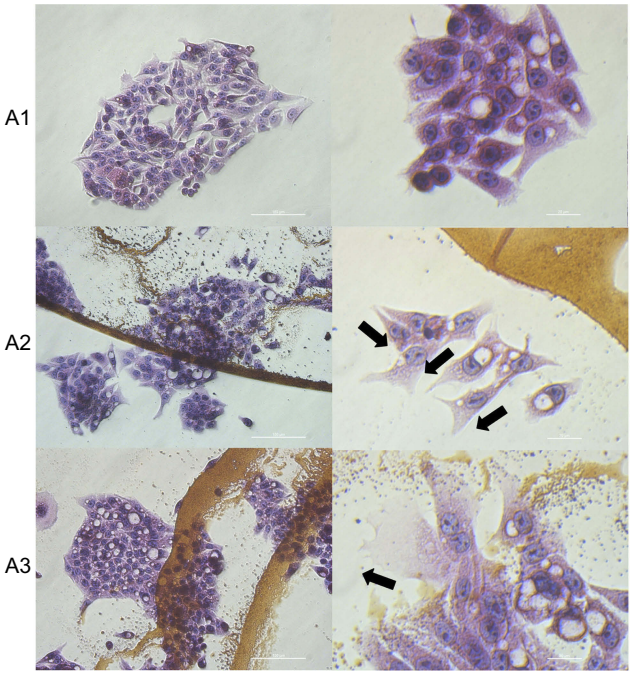

Figure 6 Morphology changes and affinity of C3A cells to the C_{60} nanofilms.
Notes: Hematoxylin-eosin staining of C3A cells on C_{60} nanofilms visualized using light optical microscopy. (**A1**) Control group; (**A2**) C_{60}-20%; and (**A3**) C_{60}-100%. Black arrows indicate the direction of cell migration. Scale bars: left pictures 100 μm, right pictures 20 μm.
Abbreviation: C_{60}, fullerenes.

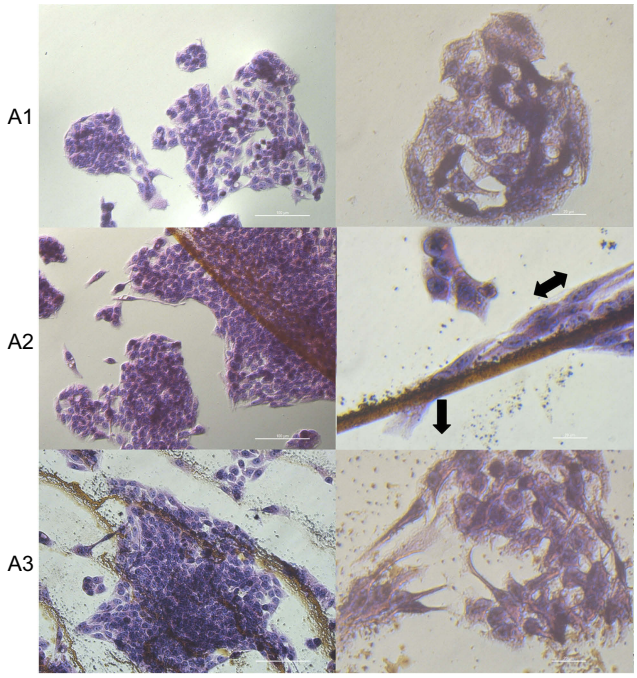

Figure 5 Morphology changes and affinity of HepG2 cells to the C_{60} nanofilms.
Notes: Hematoxylin-eosin staining of HepG2 cells on C_{60} nanofilms visualized using light optical microscopy. (**A1**) Control group; (**A2**) C_{60}-20%; and (**A3**) C_{60}-100%. Black arrows indicate the direction of cell migration. Scale bars: left pictures 100 μm, right pictures 20 μm.
Abbreviation: C_{60}, fullerenes.

HepG2 cells were touching neighboring cells, and thus filopodia and lamellipodia were unobserved (Figure 8A1 and A2). However, the preferences of the cells to the nanofilm border were observed. SEM images showed globular, round structures of HepG2 cells on C_{60} nanofilms. Generally, cell morphology was very similar to the control group on the nanofilms and their number was only slightly decreased (Figure 8A3).

Single C3A cells had lamellipodium directed toward the cell cluster and the surface of the nanofilm (Figure 9A2). Cell–cell junctions were less tight than in the control group (Figure 9A1). Cells adhered to the nanofilm by their long edges, and probably deposited more ECM components, resembling 3-D structures. Deposition of ECM provided a binding site for focal adhesions (Figure 9A2). Low magnification SEM images showed a higher number of C3A cells on C_{60} surfaces compared to the control group and other cell lines (Figure 9A3).

Elastic modulus of single cells

Cell elasticity (kPa) depends on the properties of the niche that the cells inhabit. The elastic modulus differed between cell lines and declined in the order HS-5> HepG2> C3A

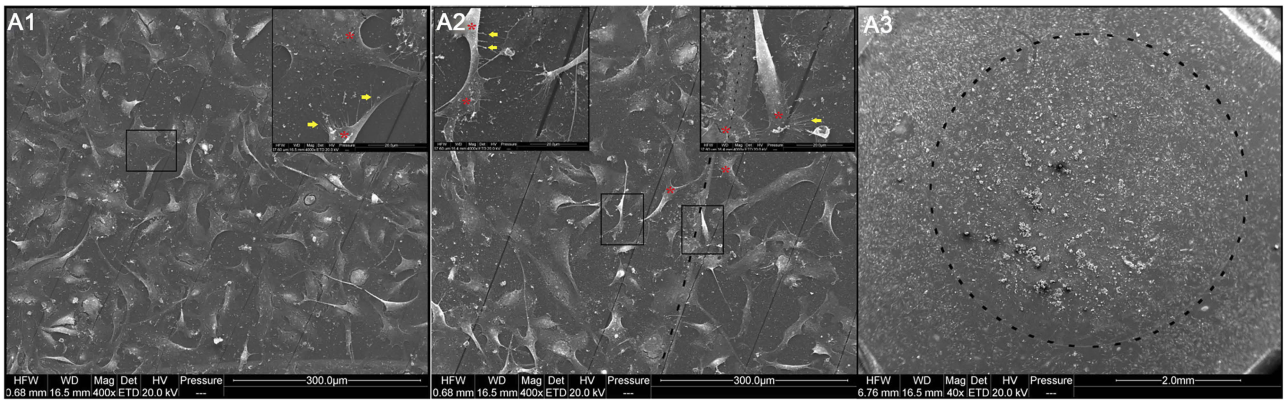

Figure 7 Visualization of the interaction of HS-5 cells with nanofilms using scanning electron microscopy.
Notes: (**A1**) Control group (**A2** and **A3**) C_{60}-20%. Red stars and yellow arrows indicate lamellipodia and filopodia, respectively. The dotted line indicates edges of the dots. Scale bars: **A1** and **A2** =300 µm and 20 µm, **A3** =2.0 mm.
Abbreviation: C_{60}, fullerenes.

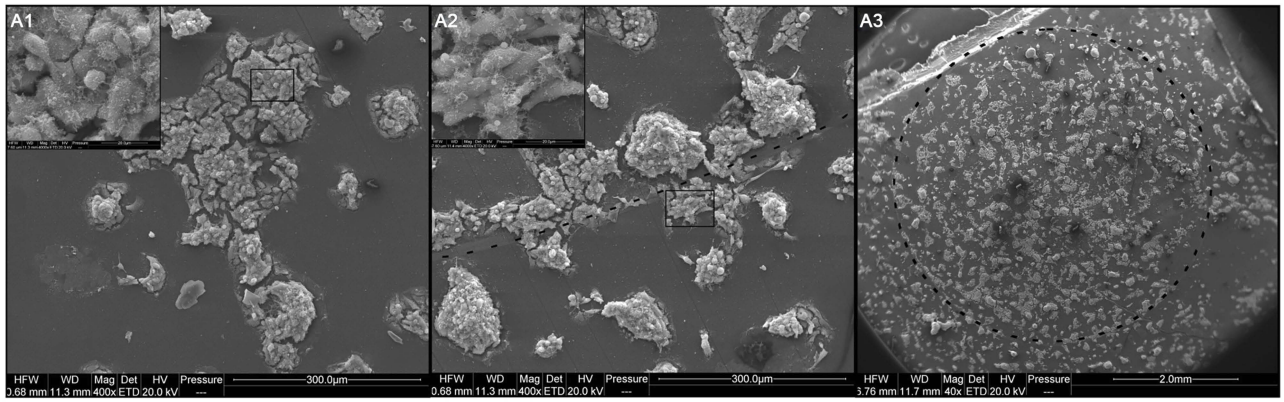

Figure 8 Visualization of the interaction of HepG2 cells with nanofilms using scanning electron microscopy.
Notes: (**A1**) Control group; (**A2** and **A3**) C_{60}-20%. The dotted line indicates edges of the dots. Scale bars: **A1** and **A2** =300 µm and 20 µm, **A3** =2.0 mm.
Abbreviation: C_{60}, fullerenes.

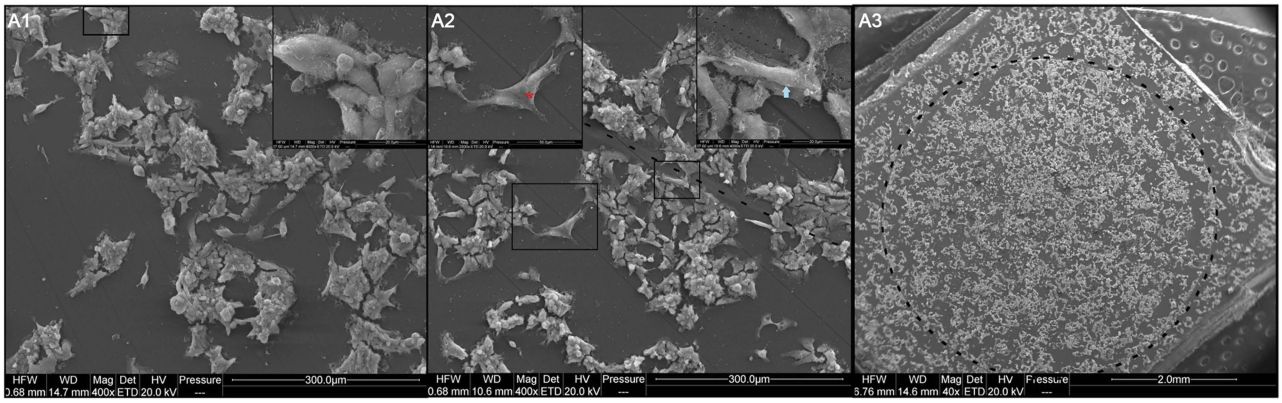

Figure 9 Visualization of the interaction of C3A cells with nanofilms using scanning electron microscopy.
Notes: (**A1**) Control group; (**A2** and **A3**) C_{60}-20%. Red and blue points indicate lamellipodia and the 3-D ECM structure, respectively. The dotted line indicates edges of the dots. Scale bars: **A1** =300 µm and 20 µm, **A2** =300 µm, 50 µm and 20 µm, **A3** =2.0 mm.
Abbreviation: C_{60}, fullerenes.

(Figure 2A). Thus, C3A cells were softer (2.24±0.4 kPa) than HS-5 (3.55±0.8 kPa) and HepG2 (3.30±1.3 kPa) cells. In addition, our studies showed softer cells on C_{60} nanofilms than on an uncoated plate (5 kPa), regardless of the cell line. Furthermore, the cell nucleus had a lower elastic modulus on C_{60} nanofilms compared to the control (Figure 2D). Regarding the cells growing on the C_{60} surface, the neighborhood of the cells was much softer than in the control cells. This may mean the deposition of biological molecules on the C_{60} surface.

Expression of integrin α5β1 and organization of the cytoskeleton

To examine the influence of nanofilms on cell adhesion, we observed the structure of the cytoskeleton and integrin α5β1 expression (Figure 10). HS-5 cells had stress fibers in the cytoplasm and short cytoskeleton protrusions (filopodia) running in parallel according to the orientation of the cells. However, growing of HS-5 on C_{60} nanofilms led to F-actin remodeling in cells and a crisscrossed pattern of the actin cytoskeleton emerged. The stress fibers ended in focal adhesion complexes—lamellipodia. We observed spread cells on C_{60} nanofilms. The HS-5 and HepG2 cultivated on C_{60} nanofilms showed intensive F-actin formation in cell cortex, suggesting the need of stabilization of cell adhesion. HS-5 cell localization and expression of integrins were significantly upregulated by the C_{60} nanofilms.

The HepG2 cells cultured on C_{60} nanofilms formed a long, thin network of protrusions, with dense cytoskeletal filaments. We observed large distances between the cells on C_{60} nanofilms for HepG2 and C3A cell lines (Figures 11 and 12). In samples growing on C_{60} nanofilms, cellular bodies of cancer liver cells showed an equal or higher expression of integrin α5β1 compared to the control. Taken together, our results indicate that C_{60} nanofilms increased contact adhesion of all three cell lines.

Effect on the cell–ECM and cell–cell connections

To determine if changes in morphology were associated with levels of cell–ECM adhesion proteins, integrin α5β1 (subsection 3.5) and vinculin were examined (Figure 3E). C_{60} nanoparticles caused a significant increase in the vinculin level of HepG2 cells (Table 1), decreased expression in HS-5 cells and did not alter expression in the C3A line (Table 2).

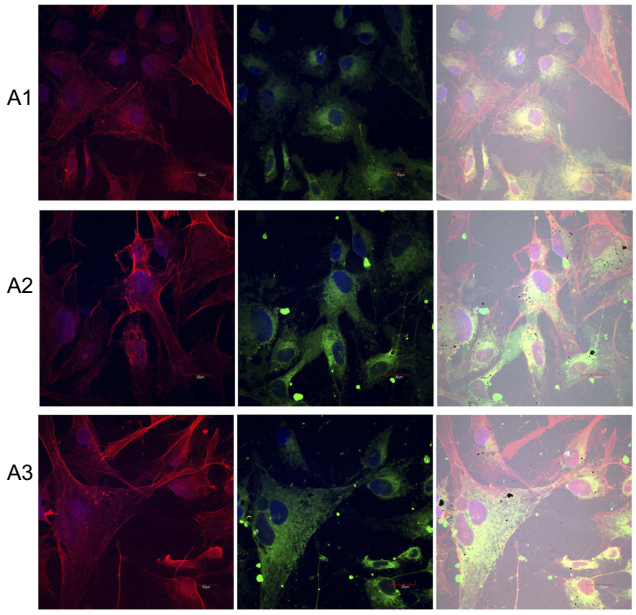

Figure 10 Expression level of integrin α5β1 and changes in cell morphology on fullerenes nanofilms.
Notes: HS-5 cells were stained with DAPI (nuclei, blue), phalloidin-Atto 633 (cytoskeleton, red) and fluorescent secondary antibody 488 FITC (integrin, green) and visualized using confocal microscopy and Nomarski interference contrast. (**A1**) Control group; (**A2**) C_{60}-20%; and (**A3**) C_{60}-100%. Scale bar: 20 μm.
Abbreviations: C_{60}, fullerenes; DAPI, 4′,6-diamidino-2-phenylindole; FITC, fluorescein isothiocyanate.

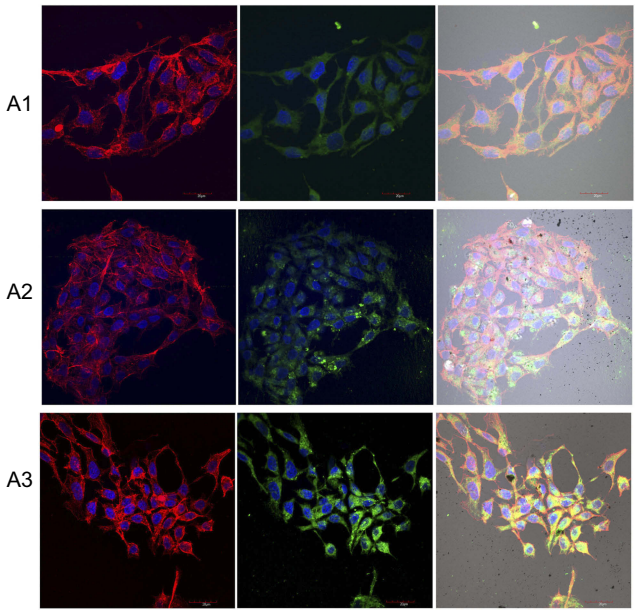

Figure 11 Expression level of integrin α5β1 and changes in cell morphology on fullerenes nanofilms.
Notes: HepG2 cells were stained with DAPI (nuclei, blue), phalloidin-Atto 633 (cytoskeleton, red) and fluorescent secondary antibody 488 FITC (integrin, green) and visualized using confocal microscopy and Nomarski interference contrast. (**A1**) Control group; (**A2**) C_{60}-20%; and (**A3**) C_{60}-100%. Scale bar: 20 μm.
Abbreviations: C_{60}, fullerenes; DAPI, 4′,6-diamidino-2-phenylindole; FITC, fluorescein isothiocyanate.

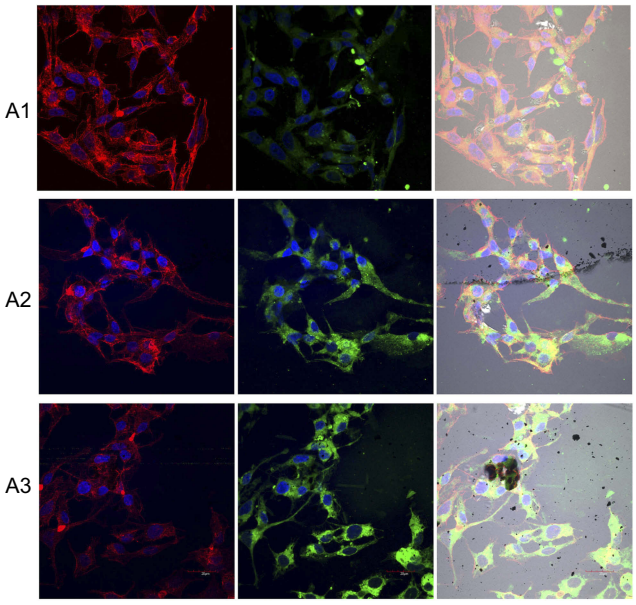

Figure 12 Expression level of integrin α5β1 and changes in cell morphology on fullerenes nanofilms.
Notes: C3A cells were stained with DAPI (nuclei, blue), phalloidin-Atto 633 (cytoskeleton, red) and fluorescent secondary antibody 488 FITC (integrin, green) and visualized using confocal microscopy and Nomarski interference contrast. (**A1**) Control group; (**A2**) C_{60}-20%; and (**A3**) C_{60}-100%. Scale bar: 20 μm.
Abbreviations: C_{60}, fullerenes; DAPI, 4′,6-diamidino-2-phenylindole; FITC, fluorescein isothiocyanate.

Table 1 Relative values of β-catenin, N-cadherin, vinculin and PCNA protein levels on C_{60} compared to the control for HepG2 cells

Adjusted density values of bands for C_{60} samples relative to the control and loading-control			ANOVA
Cell line / Protein	HepG2		SE
	C	C_{60}	
β-catenin	1	0.90	0.045
N-cadherin	1	0.73*	0.066
Vinculin	1	5.55***	0.999
PCNA	1	0.94	0.075

Note: Statistically significant differences in comparison to untreated cells (P<0.05): *P-value <0.05, **P-value <0.01, and ***P-value <0.001 (ANOVA; Dunnett's post-test). GAPDH was used as a loading control. The table presents a quantitative analysis of the pixels using ImageJ® 1.48v. Adjusted density values of bands were expressed as the relative values to the control (Area C60/Area Control), where the control value is 1. Next, bands were expressed as the relative values to the loading control (Area C60/Area Control)EP/(Area C60/Area Control)GAPDH, where EP is the examined protein (β-catenin, N-cadherin, vinculin or PCNA).
Abbreviations: ANOVA, analysis of variance; C, control group; C60, fullerenes; PCNA, Proliferating cell nuclear antigen; SE, standard error.

β-catenin and cadherin are cell–cell adhesion proteins. The intracellular distribution of proteins varied throughout each cell line. HS-5 cells had low total β-catenin expression (Table 3). Furthermore, all lines showed a decrease in β-catenin expression after 7 days of culture on C_{60} nanofilms. Similar results were obtained for N-cadherin.

Table 2 Relative values of β-catenin, N-cadherin, vinculin, and PCNA protein levels on C_{60} compared to the control for C3A cells

Adjusted density values of bands for C_{60} samples relative to the control and loading-control			ANOVA
Cell line / Protein	C3A		SE
	C	C_{60}	
β-catenin	1	0.79	0.032
N-cadherin	1	0.77	0.046
Vinculin	1	0.89	0.080
PCNA	1	1.02	0.143

Note: Statistically significant differences in comparison to untreated cells (P<0.05): *P-value <0.05, **P-value <0.01, and ***P-value <0.001. (ANOVA; Dunnett's post-test). GAPDH was used as a loading control. The table presents a quantitative analysis of the pixels using ImageJ® 1.48v. Adjusted density values of bands were expressed as the relative values to the control (Area C60/Area Control), where the control value is 1. Next, bands were expressed as the relative values to the loading control (Area C60/Area Control)EP/(Area C60/Area Control)GAPDH, where EP is the examined protein (β-catenin, N-cadherin, vinculin or PCNA).
Abbreviations: ANOVA, analysis of variance; C, control group; C60, fullerenes; PCNA, Proliferating cell nuclear antigen; SE, standard error.

Table 3 Relative values of β-catenin, N-cadherin, vinculin and PCNA protein levels on C_{60} compared to the control for HS-5 cells

Adjusted density values of bands for C_{60} samples relative to the control and loading-control			ANOVA
Cell line / Protein	HS-5		SE
	C	C_{60}	
β-catenin	1	0.31***	0.016
N-cadherin	1	0.62**	0.050
Vinculin	1	0.85	0.085
PCNA	1	0.62**	0.003

Notes: Statistically significant difference sin comparison to untreated cells (P<0.05): *P-value <0.05, **P-value <0.01, and ***P-value <0.001. (ANOVA; Dunnett's post-test). GAPDH was used as a loading control. The table presents a quantitative analysis of the pixels using ImageJ® 1.48v. Adjusted density values of bands were expressed as the relative values to the control (Area C_{60}/Area Control), where the control value is 1. Next, bands were expressed as the relative values to the loading control (Area C_{60}/Area Control)EP/(Area C_{60}/Area Control)GAPDH, where EP is the examined protein (β-catenin, N-cadherin, vinculin or PCNA).
Abbreviations: ANOVA, analysis of variance; C, control group; C_{60}, fullerenes; PCNA, Proliferating cell nuclear antigen; SE, standard error.

Cultivation on C_{60} nanofilms decreased the level of β-catenin and N-cadherin, especially in the cancer cells.

Effect on the cell cycle

To investigate if the mechanical interaction between cells and nanofilms influenced the cell cycle, flow cytometric analysis was performed (Figure 3A–D). HS-5 cells exposed to the ECM equivalent (C_{60}-100%) for 7 days showed a pronounced increase in the G2/M population, with a concomitant reduction of cells in the S and G0/G1

phases. However, in the case of HS-5 cultured on C_{60} dots, population of cells in the S and G2/M phases decreased and population of cells in the G0/G1 phase increased. Our results demonstrated that nanofilms inhibited the proliferation of cells in proportion to the surface.

As shown in Figure 3B and D, C_{60} nanofilm dots suppressed cell cycle progression in HepG2 cells. Furthermore, we observed a slight decrease in the number of HepG2 cells in the S phase and an increase in the number of cells in the G2/M phase following the C_{60}-20% nanofilm application. These results indicated that the anti-proliferative effect of the C_{60} surface is associated with an arrest in G2/M phase of the cell cycle.

C3A cells were the least sensitive to cell cycle arrest by C_{60} nanofilms, which was consistent with other measurements (Figure 3C and D).

Discussion

The objective of this study was to explain whether fullerenes could serve as a potential component of the ECM, as allowing its revitalization will affect the reduction of malignancy of tumor cells, particularly, the inhibition of the rate of their proliferation and change of the cell cycle. We hypothesized that C_{60} fullerenes nanofilms would optimize the mechanical properties of the microenvironment of liver cancer cells, and through mechanotransduction, affect the normalization of cell behavior.

However, the fundamental issue in forcing cancer cells to decrease their proliferation rate is to create a non-toxic, biocompatible and pro-adhesive nanomaterial that will change their behavior to follow that of normal division. For this purpose, we analyzed the effect of a potent component of the ECM (self-organized C_{60} nanofilm) on biocompatibility and the affinity of cells to the nanofilm.

In in vitro studies, the biocompatibility of the nanostructures or the affinity of cells to the nanostructures has usually been assessed by introducing nanoparticles to the cells at increasing concentrations or by the cultivation of cells on the examined surface.[53] This procedure does not allow the evaluation of affinity, because we do not observe preferences in the natural migration of the cells to the nanomaterial. Herein, we use a rapid method described by Sawosz et al[46] to increase the reliability of measurements, using the C_{60} nanofilm dots pattern (Figure 1A). We investigated the behavior of cells on the surface covered with nanofilms as well as on the surface covered by dots. Nanofilm as a layer has a larger particles size, which makes it difficult to enter the cell. Additionally, the fullerene solubility is very weak and requires sonication several times. The present study showed that the C_{60} nanofilm was strongly bound to the polystyrene plate. Preliminary results did not show pores in the cell membrane. However, the localization of fullerene requires further studies by C_{60}-fluorophore conjugated or transmission electron microscopy.

The external physical forces and chemical signals perceived by the cells determine the cell affinity to the nanofilms.[54] All cell lines used did spread on the C_{60} nanofilms and showed high affinity to the nanofilm border. HS-5 cells migrated along the long axis and extended lamellipodium and numerous filopodia. The individual HepG2 and C3A cells migrated toward the surface of C_{60} nanofilm and created cell clusters. In the clusters, the cells were preferentially located on the border and surface of C_{60} nanofilm. Moreover, no dead cells were observed that lost their adherence,[54] which would suggest a lack of affinity. Visualization of cells on the C_{60} surface and dots indicated the cell affinity to and the preferential colonization of cells on the nanofilms and may point to C_{60} possibly being a beneficial component of an artificial ECM.

The ECM is a mosaic of various proteins, saccharides and other compounds,[13] not a homogeneous platform, so cells may prefer a differentiated part of the pseudo-ECM matrix, in this case, the border between the nanofilm and plastic. A similar methodology was used by Lunova et al, where HepG2 cells seeded on silicon substrates with circular, square and striped pillars, with 50 μm spacing, showed higher growth rates than those with 500 μm spacing.[55]

Morphological examination confirmed that cells preferred C_{60} over the uncoated plate. This may result from the physical properties of this nanomaterial (sp^2 carbon hybridisation). Moreover, C_{60} has anionic charges like the major constituents of the ECM's acidic molecules.[56] Also, Tatur et al reported that functionalization of nanoparticles with cationic groups caused the nanoparticles to have a tendency to penetrate the lipid membrane of cells.[57] Furthermore, the geometric structure of the examined nanomaterial might influence adhesion, thus C_{60}, as the symmetric molecule with a soccer ball shape,[58] was a preferable niche. Kopova et al demonstrated that substrates with nanoscale irregularities also promote the adsorption of cell adhesion proteins (eg, fibronectin, vitronectin) present in the serum of the culture media.[59] Thus, the higher roughness of C_{60} surface (161 nm) than the uncoated plate (5 nm) promoted cell adhesion.[60] The morphology confirmed that cells observed on the C_{60} nanofilms (20% and 100%) looked

normal; moreover, C3A cells were located preferentially on C_{60} dots. Furthermore, C_{60} nanofilms did not cause the formation of spheroids, suggesting the lack of tendency to change the transit from a single cell to collective invasion strategies of mesenchymal cancer cells.[61]

The perfect niche should be non-toxic, biocompatible and promote good adhesion for normal and cancer cells.[19] Carbon nanomaterials seem to be very promising because of their moderate toxicity. However, depending on the type of allotrope, their size, shape or the functional groups available at the surface, the in vitro toxicity differs. The evaluation of cell viability indicated that the toxicity of C_{60} declined in the order HS-5> HepG2> C3A. According to the manufacturer's data, C3A is a clonal derivative of HepG2 that was selected for the high albumin production, high production of alpha-fetoprotein (AFP) and ability to grow in glucose-deficient medium. These features of C3A cells cause higher resistance to treatment than HepG2 cell line. Marchesan et al reported that the main difficulty in applying carbon-based materials in clinical settings is their biodistribution and the formation of the protein corona. The blood plasma proteins adsorb to nanoparticles surface and form protein corona.[62] Thus, albumins and AFP from C3A and HepG2 cells can change the interaction of nanoparticles with cells and mitigates their cytotoxicity via modulating nanoparticles physicochemical properties.[63] Thus, liver cells synthesize a lot of proteins and form the protein corona, which means that the impact of nanoparticles is smaller. Moreover, normal HS-5 cells were more mechanosensitive, and their metabolic activity was decreased. Hepatocytes as detoxifying and highly metabolically active cells are more resistance than HS-5 cells after treatment. Thus, hepatocytes responsible for drug and toxin metabolism, and their accumulation is naturally less sensitive. The present results are in line with studies with different types of cancer cells that demonstrated a slight decrease in cell viability using C_{60}.[32–34,38–40]

Young's modulus values are different in various cell regions. For example, the cell nucleus is relatively soft compared to the entire cell. However, C_{60} surface caused the elasticity of the nucleus to be softer and easier to deform. Liu et al showed significant alterations in the elastic moduli between the control SMCC-7721 cells and fullerenol $C_{60}(OH)_{24}$-treated cells.[64] Similar to our results, after treatment with C_{60}, the elastic modulus decreased and the average height of SMCC-7721 cells increased. Thus, cells were softer than in the control group, which resembled the normal liver cell phenotype. The decrease in the average elastic modulus could be caused by the remodeling of actin filaments, which play an important role in the cell's mechanical stability.[64] In the experiments conducted for this study, we wanted to confirm the influence of mechanical stimuli on the remodeling of cytoskeleton and proliferation.

Our results suggest that C_{60} is a compatible and suitable ECM substitute which may attract cancer cells and change their adhesion. We expected that it should be reflected by the expression of integrin receptors, especially α5β1, playing an intermediary role between cells and the ECM.

Data from previous reports support a correlation between nanofilm properties—stiffness and metastases, extension and expansion morphology—and the delay of the S phase of the cell cycle.[65] In a key experiment, Wu et al demonstrated that the integrin β1/α5/JNK/c-JUN signaling pathway is regulated by matrix stiffness.[14] A higher stiffness induced LOXL2 upregulation in HCC cells and the recruitment of bone marrow-derived cells to assist a premetastatic niche formation. Morozevich et al demonstrated that integrin α5β1 depletion of MCF-7Dox (human breast carcinoma cells) decreased MMP-2 collagenase expression and tumor progression.[66] Thus, downregulation of integrin α5β1 seemed to promote weak cell adhesion, proliferation and metastasis by decreasing p21 and p27 protein levels (cyclin-dependent kinase inhibitor), activating p300-mediated histone acetylation and recruiting the Sp1 transcriptional factor.[67,68] The results of a recent study indicated that the β1 subunit, in combination with αv subunit of integrins, played a key role in excessive liver fibrosis via transforming growth factor-β1 (TGFβ1) signaling.[69] We suggest that manipulating the stiffness and roughness of the microenvironment can change integrin expression, as a reaction to a mechanical signal.

Stimuli of a mechanical nature from a nanofilm (compressive, tensile or shear stress) are received via the cells' integrins.[65] In our study, C_{60} increased the expression of the α5β1 integrin protein in cancer cells. Moreover, the distribution and expression of this integrin varied considerably between the type of cells, being greater for normal (HS-5) and smaller for cancer cells (HepG2, C3A). Given that the expression of the α5β1 integrin in HCC is lower than in normal hepatocytes[68] and that C_{60} surfaces increased integrin expression preferentially for cancer cells, we suspect that the C_{60} nanofilm effect may restore a normal status of HCC. Consequences of the nanofilm-integrin mechanism of stimuli were also confirmed by visualization of the cell morphology. Cells grown on

C_{60}-coated dishes displayed the largest cell spreading areas and the greatest sizes and numbers of focal adhesions, which is involved in the mechanotransduction pathway.[70] C_{60}, not used as a nanofilm but administered into the medium (200 μg/mL), did not alter the cytoskeletal organization of normal (MCF10A) and malignant (MDA-MB 435, MDA-MB 231, HepG2) cells,[71] indicating that the surface-imitating niche, but not nanostructures suspended in the medium, transmits the mechanosignals to the cell. However, due to the specificity of liver cells, such as rapid growth as clusters, actin filaments are difficult to observe in single cells.[72] Upon ligand occupancy and during the organization of the focal adhesion complex, the cytoskeleton is reorganized.[73,74] The transduction of the signal from integrins to the cytoskeleton affects the behavior of the cell, for example, migration, adhesion and proliferation.[75] Moreover, integrins seem to be the major mechanoreceptors in interacting cell–ECM components, initiating biochemical signaling and protecting against a metastatic phenotype.[14,65,76]

Considering the observed changes in the cytoskeleton and cell–cell contacts, we investigated whether such changes also affect the expression of major proteins, such as vinculin, β-catenin and N-cadherin. The decrease in β-catenin levels weakens the tight connections between cells as observed for liver cells.[77,78] According to Lee et al, strengthening one type of adhesion (ECM-integrin-vinculin) opposes the formation of the other in an antagonistic manner (E-cadherin-β-catenin).[54] β-catenin may also accumulate in the nucleus and thereby reduce cell proliferation. Wierzbicki et al demonstrated that pristine graphene and graphene oxide nanoparticles can decrease the β-catenin level in the nuclear fraction via the EGFR/AKT/mTOR and the β-catenin pathways. These pathways decreased the invasiveness and migration of U87 and U118.[47] Treatment with C_{60} caused reduced levels of N-cadherin and an increase of vinculin expression. This suggests that cell–ECM connections protect against migration.[21,79]

In our study, we found that carbon nanofilms mimicked the niche of cells, were biocompatible, nontoxic and simultaneously inhibited proliferation of HCC cells. This biocompatible nanofilm decreased PCNA expression—a molecular marker of proliferation. Some studies revealed specific peptides interacting with PCNA in the nucleus and showed antiproliferative effects were a signal to block cell cycle progression.[80] Moreover, it was shown that overexpression of the integrin β1 subunit induced S phase delay and inhibited SMMC-7721 cell proliferation.[81]

The matrix compliance regulates cell cycle by changes in cell shape. The cell shape is associated with the cell cycle phase, for example, cell rounding heralds the start of mitosis.[82] Regulation of the G1/S and G2/M transition is implicated in many cancers including HCC. In hepatoma cells, some transcripts (suppressor proteins) are upregulated or downregulated, changing the cell-cycle distribution, namely the G0/G1, S and G2/M phases. Cells cannot progress through G1 into S phase in the absence of integrin signaling. Integrin-mediated adhesion activates Rho GTPases and causes loss of cell-cycle inhibitors.[82] Formation of HCC is associated with bypassing the detection of DNA damage and proliferation of defective cells. Non-tumor cells with damaged DNA do not transition from the G2 phase to mitosis. However, the cancer chromosomes can bypass the DNA damage detection checkpoint, such as G2/M. Shi et al showed that destruction of Cyclin A and inactivation of CycA/cyclin-dependent kinases 1 allow the cell cycle arrest in G2/M phase, which is not observed in cancer cells.[83] This type of regulation is critical to prevent normal cells from going through malignant transformation.[82,83]

In the present study, flow cytometric analysis showed that the cell cycle of HepG2 and HS-5 cells was arrested by C_{60} at the G2 (preparation to divide) and M (cell division) phases, accompanied by a decreased cell number at S phase. In our experiments, C3A cells were the least sensitive to cell cycle arrest by carbon nanofilms. The results indicate that the C_{60} nanofilm might be an attractive mechanical, substitute niche for HCC by colonizing and limiting cell division without inducing toxicity.[34] All these data indicated that fullerenes triggered G2/M-phase arrest by mechanotransduction towards membrane proteins, cytoskeleton and the nucleus.

Conclusion

The physical structure of the ECM surface is, alongside chemical factors, a fundamental signaling structure. In studies on liver cancer cells, we documented that the signal derived from the fullerene nanofilm is preferentially chosen by the cell, creating an environment conducive to adhesion and colonization. Furthermore, cells settled in this way decreased the ability to form spheroids, caused the cell cycle arrest in the G2/M phase and decreased proliferation. It can be expected that the incorporation of fullerenes in the ECM of liver cancer cells can reduce cell malignancy and improve tumor therapy.

Acknowledgments

This research was carried out in the framework of the National Science Centre Poland Project, number 2016/21/B/NZ9/01029. This report is a part of Malwina Sosnowska's PhD thesis.

Author contributions

All authors contributed towards data analysis, drafting and critically revising the paper, gave final approval of the version to be published, and agreed to be accountable for all aspects of the work.

Disclosure

The authors report no conflicts of interest in this work.

References

1. Schrader J, Gordon-Walker TT, Aucott RL, et al. Matrix stiffness modulates proliferation, chemotherapeutic response, and dormancy in hepatocellular carcinoma cells. *Hepatology*. 2011;53(4):1192–1205. doi:10.1002/hep.24108
2. Mittal S, El-Serag HB. Epidemiology of HCC: consider the population. *J Clin Gastroenterol*. 2013;47:S2–S6. doi:10.1097/MCG.0b013e3182872f29
3. Yau WL, Lam CSC, Ng L, et al. Over-expression of miR-106b promotes cell migration and metastasis in hepatocellular carcinoma by activating epithelial-mesenchymal transition process. *PLoS One*. 2013;8(3):e57882. doi:10.1371/journal.pone.0057882
4. Wai CT, Greenson JK, Fontana RJ, et al. A simple non-invasive index can predict both significant fibrosis and cirrhosis in patients with chronic hepatitis C. *Hepatology*. 2003;38(2):518–526. doi:10.1053/jhep.2003.50346
5. Wynn TA, Ramalingam TR. Mechanisms of fibrosis: therapeutic translation for fibrotic disease. *Nat Med*. 2012;18(7):1028–1040. doi:10.1038/nm.2807
6. Baiocchini A, Montaldo C, Conigliaro A, et al. Extracellular matrix molecular remodeling in human liver fibrosis evolution. *PLoS One*. 2016;11(3):e0151736. doi:10.1371/journal.pone.0151736
7. Haase K, Pelling AE. Investigating cell mechanics with atomic force microscopy. *J R Soc Interface*. 2015;12(104):20140970. doi:10.1098/rsif.2014.0970
8. Gao J, Rong Y, Huang Y, et al. Cirrhotic stiffness affects the migration of hepatocellular carcinoma cells and induces sorafenib resistance through YAP. *J Cell Physiol*. 2018;234(3):2639–2648. doi:10.1002/jcp.27078
9. Li QS, Lee GY, Ong CN, Lim CT. AFM indentation study of breast cancer cells. *Biochem Biophys Res Commun*. 2008;374(4):609–613. doi:10.1016/j.bbrc.2008.07.078
10. Lekka M, Gil D, Pogoda K, et al. Cancer cell detection in tissue sections using AFM. *Arch Biochem Biophys*. 2012;518(2):151–156. doi:10.1016/j.abb.2011.12.013
11. Samani A, Zubovits J, Plewes D. Elastic moduli of normal and pathological human breast tissues: an inversion-technique-based investigation of 169 samples. *Phys Med Biol*. 2007;52(6):1565–1576. doi:10.1088/0031-9155/52/6/002
12. Provenzano PP, Inman DR, Eliceiri KW, et al. Collagen density promotes mammary tumor initiation and progression. *BMC Med*. 2008;6(1):11. doi:10.1186/1741-7015-6-11
13. Parekh A, Weaver AM. Regulation of cancer invasiveness by the physical extracellular matrix environment. *Cell Adh Migr*. 2009;3(3):288–292. doi:10.4161/cam.3.3.8888
14. Wu S, Zheng Q, Xing X, et al. Matrix stiffness-upregulated LOXL2 promotes fibronectin production, MMP9 and CXCL12 expression and BMDCs recruitment to assist pre-metastatic niche formation. *J Exp Clin Cancer Res*. 2018;37(1):99. doi:10.1186/s13046-018-0761-z
15. Breuls RGM, Jiya TU, Smit TH. Scaffold stiffness influences cell behavior: opportunities for skeletal tissue engineering. *Open Orthop J*. 2008;2:103–109. doi:10.2174/1874325000802010103
16. Mitra AK, Sawada K, Tiwari P, Mui K, Gwin K, Lengyel E. Ligand-independent activation of c-Met by fibronectin and $\alpha_5\beta_1$-integrin regulates ovarian cancer invasion and metastasis. *Oncogene*. 2011;30(13):1566–1576. doi:10.1038/onc.2010.532
17. Murke F, Vitorianoda CC, Giebel B, Görgens A. Concise review: asymmetric cell divisions in stem cell biology. *Symmetry*. 2015;7(4):2025–2037. doi:10.3390/sym7042025
18. Lu P, Weaver VM, Werb Z. The extracellular matrix: a dynamic niche in cancer progression. *J Cell Biol*. 2012;196(4):395–406. doi:10.1083/jcb.201102147
19. Lechler T, Fuchs E. Asymmetric cell divisions promote stratification and differentiation of mammalian skin. *Nature*. 2005;437(7056):275–280. doi:10.1038/nature03922
20. Lee M, Vasioukhin V. Cell polarity and cancer—cell and tissue polarity as a non-canonical tumor suppressor. *J Cell Sci*. 2008;121(8):1141–1150. doi:10.1242/jcs.018713
21. Yang JD, Nakamura I, Roberts LR. The tumor microenvironment in hepatocellular carcinoma: current status and therapeutic targets. *Semin Cancer Biol*. 2011;21(1):35–43. doi:10.1016/j.semcancer.2010.10.007
22. Deakin NO, Turner CE. Paxillin comes of age. *J Cell Sci*. 2008;121(15):2435–2444. doi:10.1242/jcs.018713
23. Cho S, Irianto J, Discher DE. Mechanosensing by the nucleus: from pathways to scaling relationships. *J Cell Biol*. 2017;216(2):305–315. doi:10.1083/jcb.201610042
24. Elosegui-Artola A, Andreu I, Beedle AEM, et al. Force triggers YAP nuclear entry by regulating transport across nuclear pores. *Cell*. 2017;171(6):1397–1410. doi:10.1016/j.cell.2017.10.008
25. Geiger B, Yamada KM. Molecular architecture and function of matrix adhesions. *Cold Spring Harb Perspect Biol*. 2011;3(5):a005033. doi:10.1101/cshperspect.a005033
26. Tilghman RW, Cowan CR, Mih JD, et al. Matrix rigidity regulates cancer cell growth and cellular phenotype. *PLoS One*. 2010;5(9):e12905. doi:10.1371/journal.pone.0012905
27. Wong S, Guo WH, Wang YL. Fibroblasts probe substrate rigidity with filopodia extensions before occupying an area. *Proc Natl Acad Sci USA*. 2014;111(48):17176–17181. doi:10.1073/pnas.1412285111
28. Yamaguchi H, Condeelis J. Regulation of the actin cytoskeleton in cancer cell migration and invasion. *Biochim Biophys Acta*. 2007;1773(5):642–652. doi:10.1016/j.bbamcr.2006.07.001
29. Yamaguchi H, Oikawa T. Membrane lipids in invadopodia and podosomes: key structures for cancer invasion and metastasis. *Oncotarget*. 2010;1(5):320–328. doi:10.18632/oncotarget.v1i5
30. Abarrategi A, Gutiérrez MC, Moreno-Vicente C, et al. Multi-wall carbon nanotube scaffolds for tissue engineering purposes. *Biomaterials*. 2008;29(1):94–102. doi:10.1016/j.biomaterials.2007.09.021
31. Kumar R, Raza K. C_{60} fullerenes as drug delivery carriers for anticancer agents: promises and hurdles. *Pharm Nanotechnol*. 2017;5(3):169–179.
32. Kolosnjaj J, Szwarc H, Moussa F. Toxicity studies of fullerenes and derivatives. *Adv Exp Med Biol*. 2007;620:168–180.
33. Sun C, Wang L, Gao D, et al. $C_{60}(OH)_{22}$: a potential histone deacetylase inhibitor with anti-angiogenic activity. *Nanoscale*. 2016;8(36):16332–16339. doi:10.1039/c6nr04875g
34. Prylutska S, Politenkova S, Afanasieva K, et al. A nanocomplex of C_{60} fullerene with cisplatin: design, characterization, and toxicity. *Beilstein J Nanotechnol*. 2017;8(1):1494–1501. doi:10.3762/bjnano.8.149
35. Prylutska S, Grynyuk I, Matyshevska O, et al. C_{60} fullerene as synergistic agent in tumor-inhibitory doxorubicin treatment. *Drugs R D*. 2014;14(4):333–340. doi:10.1007/s40268-014-0074-4

36. Mori TT, Takada H, Ito S, Matsubayashi K, Miwa N, Sawaguchi T. Preclinical studies on safety of fullerene upon acute oral administration and evaluation for no mutagenesis. *Toxicology*. 2006;225(1):48–54. doi:10.1016/j.tox.2006.05.001
37. Hendrickson OD, Zherdev AV, Gmoshinskii IV, Dzantiev BB. Fullerenes: in vivo studies of biodistribution, toxicity, and biological action. *Nanotechnol Russ*. 2014;9(11–12):601–617. doi:10.1134/S199507801406010X
38. Injac R, Perse M, Obermajer N, et al. Potential hepatoprotective effects of fullerenol $C_{60}(OH)_{24}$ in doxorubicin-induced hepatotoxicity in rats with mammary carcinomas. *Biomaterials*. 2008;29(24–25):3451–3460. doi:10.1016/j.biomaterials.2008.04.048
39. Tolkachov M, Sokolova V, Loza K, et al. Study of biocompatibility effect of nanocarbon particles on various cell types *in vitro*. *Mat-Wiss U Werkstofftech*. 2016;47(2–3):216–221. doi:10.1002/mawe.201600486
40. Baati T, Bourasset F, Gharbi N, et al. The prolongation of the lifespan of rats by repeated oral administration of [60]fullerene. *Biomaterials*. 2012;33(19):4936–4946. doi:10.1016/j.biomaterials.2012.03.036
41. Harhaji L, Isakovic A, Reicevic N, et al. Multiple mechanisms underlying the anticancer action of nanocrystalline fullerene. *Eur J Pharmacol*. 2007;568(1–3):89–98. doi:10.1016/j.ejphar.2007.04.041
42. Franskevych D, Palyvoda K, Petukhov D, et al. Fullerene C_{60} penetration into leukemic cells and its photoinduced cytotoxic effects. *Nanoscale Res Lett*. 2017;12(1):40. doi:10.1186/s11671-016-1819-5
43. Raoof M, Mackeyev Y, Cheney MA, Wilson LJ, Curley SA. Internalization of C_{60} fullerenes into cancer cells with accumulation in the nucleus via the nuclear pore complex. *Biomaterials*. 2012;33(10):2952–2960. doi:10.1016/j.biomaterials.2011.12.043
44. Salonen E, Lin S, Reid ML, et al. Real-time translocation of fullerene reveals cell contraction. *Small*. 2008;4(11):1986–1992. doi:10.1002/smll.200701279
45. Sawosz E, Chwalibog A, Szeliga J, et al. Visualization of gold and platinum nanoparticles interacting with *Salmonella Enteritidis* and *Listeria monocytogenes*. *Int J Nanomed*. 2010;5:631–637.
46. Sawosz E, Grodzik M, Hotowy A, et al. Warsaw University of Life Sciences. The method of multilateral assessment of biocompatibility of materials. Poland patent 423414. 2017 Nov 10.
47. Wierzbicki M, Jaworski S, Kutwin M, et al. Diamond, graphite, and graphene oxide nanoparticles decrease migration and invasiveness in glioblastoma cell lines by impairing extracellular adhesion. *Int J Nanomed*. 2017;12:7241–7254. doi:10.2147/IJN.S146193
48. Zgłobicka I, Chlanda A, Woźniak M, et al. Microstructure and nanomechanical properties of single stalks from diatom *Didymosphenia geminata* and their change due to adsorption of selected metal ions. *J Phycol*. 2017;53(4):880–888. doi:10.1111/jpy.12548
49. Dulińska M, Targosz W, Strojny W, et al. Stiffness of normal and pathological erythrocytes studied by means of atomic force microscopy. *J. Biochem Biophys Methods*. 2006;66(1–3):1–11. doi:10.1016/j.jbbm.2005.11.003
50. https://medschool.ucsd.edu, UC San Diego, Health Sciences, California, USA. Cell cycle analysis by DNA content (propidium iodide). Available from: https://healthsciences.ucsd.edu/research/moores/shared-resources/flow-cytometry/protocols/Pages/cell-cycle-with-pi.aspx. Accessed July 17, 2018
51. Saeedfar K, Heng LY, Ling TL, Rezayi M. Potentiometric urea biosensor based on an immobilized fullerene–urease bio-conjugate. *Ah S Sens*. 2013;13(12):16851–16866. doi:10.3390/s131216851
52. Chen B, Kumar G, Co CC, Ho CC. Geometric control of cell migration. *Sci Rep*. 2013;3:2827. doi:10.1038/srep02827
53. Jaworski S, Sawosz E, Grodzik M, et al. In vitro evaluation of the effects of graphene platelets on glioblastoma multiforme cells. *Int J Nanomed*. 2013;8:413–420.
54. Lee JH, Kim DH, Lee HH, Kim HW. Role of nuclear mechanosensitivity in determining cellular responses to forces and biomaterials. *Biomaterials*. 2019;197:60–71. doi:10.1016/j.biomaterials.2019.01.010
55. Lunova M, Zablotskii V, Dempsey NM, et al. Modulation of collective cell behaviour by geometrical constraints. *Integr Biol*. 2016;8(11):1099–1110. doi:10.1039/C6IB00125D
56. Theocharis AD, Skandalis SS, Gialeli C, Karamanos NK. Extracellular matrix structure. *Adv Drug Deliv Rev*. 2016;97:4–27. doi:10.1016/j.addr.2015.11.001
57. Tatur S, Maccarini M, Barker RD, Nelson A, Fragneto G. Effect of functionalized gold nanoparticles on floating lipid bilayers. *Langmuir*. 2013;29(22):6606–6614. doi:10.1021/la401074y
58. Yadav BC, Kumar R. Structure, properties, and applications of fullerenes. *Int J Nanotechnol APP*. 2008;2(1):15–24.
59. Kopova I, Bacakova L, Lavrentiev V, Vacik J. Growth and potential damage of human bone-derived cells on fresh and aged fullerene C_{60} films. *Int J Mol Sci*. 2013;14(5):9182–9204. doi:10.3390/ijms14059182
60. Gatoo MA, Naseem S, Arfat MY, Mahmood Dar A, Qasim K, Zubair S. Physicochemical properties of nanomaterials: implication in associated toxic manifestations. *Biomed Res Int*. 2014;2014:498420.
61. Haeger A, Krause M, Wolf K, Friedl P. Cell jamming: collective invasion of mesenchymal tumor cells imposed by tissue confinement. *Biochim Biophys Acta*. 2014;1840(8):2386–2395. doi:10.1016/j.bbagen.2014.03.020
62. Marchesan S, Melchionna M, Prato M. Carbon nanostructures for nanomedicine: opportunities and challenges. *Fuller Nanotub Car N*. 2014;22(1–3):190–195. doi:10.1080/1536383X.2013.798726
63. Nguyen VH, Meghani NM, Amin HH, et al. Modulation of serum albumin protein corona for exploring cellular behaviors of fattigation-platform nanoparticles. *Colloid Surface B*. 2018;170:179–186. doi:10.1016/j.colsurfb.2018.05.060
64. Liu Y, Wang Z, Wang X. AFM-based study of fullerenol $(C_{60}(OH)_{24})$-induced changes of elasticity in living SMCC-7721 cells. *J Mech Behav Biomed*. 2015;45:65–74. doi:10.1016/j.jmbbm.2014.12.011
65. Dong Y, Xie X, Wang Z, et al. Increasing matrix stiffness upregulates vascular endothelial growth factor expression in hepatocellular carcinoma cells mediated by integrin β1. *Biochem Bioph Res Commun*. 2014;444(3):427–432. doi:10.1016/j.bbrc.2014.01.079
66. Morozevich G, Kozlova N, Cheglakov I, Ushakova N, Integrin BA. α5β1 controls invasion of human breast carcinoma cells by direct and indirect modulation of MMP-2 collagenase activity. *Cell Cycle*. 2009;8(14):2219–2225. doi:10.4161/cc.8.14.8980
67. Wu Y, Qiao X, Qiao S, Yu L. Targeting integrins in hepatocellular carcinoma. *Expert Opin Ther Targets*. 2011;15(4):421–437. doi:10.1517/14728222.2011.555402
68. Fu Y, Fang Z, Liang Y, et al. Overexpression of integrin β1 inhibits proliferation of hepatocellular carcinoma cell SMMC-7721 through preventing Skp2-dependent degradation of p27 via PI3K pathway. *J Cell Biochem*. 2007;102(3):704–718. doi:10.1002/jcb.21323
69. Reed NI, Chen C, Tsujino K, Arnold TD, DeGrado WF, Sheppard D. The αvβ1 integrin plays a critical in vivo role in tissue fibrosis. *Sci Transl Med*. 2015;7(288):288ra79–288ra79. doi:10.1126/scitranslmed.aaa5094
70. Yeh YC, Ling JY, Chen WC, Lin HH, Tang MJ. Mechanotransduction of matrix stiffness in regulation of focal adhesion size and number: reciprocal regulation of caveolin-1 and β1 integrin. *Sci Rep*. 2017;7(1):15008. doi:10.1038/s41598-017-14932-6
71. Levi N, Hantgan RR, Lively MO, Caroll DL, Prasad GL. C_{60} fullerenes: detection of intracellular photoluminescence and lack of cytotoxic effects. *J Nanobiotechnol*. 2006;4(1):1–11. doi:10.1186/1477-3155-4-14
72. Sun H, Tang H, Xie D, et al. Krüppel-like factor 4 blocks hepatocellular carcinoma dedifferentiation and progression through activation of hepatocyte nuclear factor-6. *Clin Cancer Res*. 2016;22(2):502–512. doi:10.1158/1078-0432.CCR-16-0190
73. Su JM, Gui L, Zhou YP, Zha XL. Expression of focal adhesion kinase and α5 and β1 integrins in carcinomas and its clinical significance. *World J Gastroenterol*. 2002;8(4):613–618. doi:10.3748/wjg.v8.i4.613

74. Wu Y, Zuo J, Ji G, et al. Proapoptotic function of integrin β_3 in human hepatocellular carcinoma cells. *Clin Cancer Res*. 2009;15(1):60–69. doi:10.1158/1078-0432.CCR-09-0547
75. Kim SH, Turnbull J, Guimond S. Extracellular matrix and cell signaling: the dynamic cooperation of integrin, proteoglycan, and growth factor receptor. *J Endocrinol*. 2011;209(2):139–151. doi:10.1530/JOE-10-0377
76. Nowakowska A, Tarasiuk J. Procesy inwazji I przerzutowania komórek nowotworowych opornych na chemioterapię. *Postepy Hig Med Dosw*. 2017;71:380–397.
77. Wang W, Wen Q, Luo J, et al. Suppression of β-catenin nuclear translocation by CGP57380 decelerates poor progression and potentiates radiation-induced apoptosis in nasopharyngeal carcinoma. *Theranostics*. 2017;7(7):2134–2149. doi:10.7150/thno.17665
78. Khalaf AM, Fuentes D, Morshid AI, et al. Role of Wnt/β-catenin signaling in hepatocellular carcinoma, pathogenesis, and clinical significance. *J Hepatocell Carcinoma*. 2018;5:61. doi:10.2147/JHC.S156701
79. Huang DL, Bax NA, Buckley CD, Weis WI, Dunn AR. Vinculin forms a directionally asymmetric catch bond with F-actin. *Science*. 2017;357(6352):703–706. doi:10.1126/science.aan2556
80. Ling X, Kamangar S, Boytim ML, et al. Proliferating cell nuclear antigen as the cell cycle sensor for an HLA-derived peptide blocking T cell proliferation. *J Immunol*. 2000;164(12):6188–6192. doi:10.4049/jimmunol.164.12.6188
81. Liang YL, Lei TW, Wu H, et al. S-phase delay in human hepatocellular carcinoma cells induced by overexpression of integrin β1. *World J Gastroenterol*. 2003;9(8):1689–1696. doi:10.3748/wjg.v9.i8.1689
82. Provenzano PP, Keely PJ. Mechanical signaling through the cytoskeleton regulates cell proliferation by coordinated focal adhesion and Rho GTPase signaling. *J Cell Sci*. 2011;124(8):1195–1205. doi:10.1242/jcs.067009
83. Shi J, Ye G, Zhao G, et al. Coordinative control of G2/M phase of the cell cycle by non-coding RNAs in hepatocellular carcinoma. *PeerJ*. 2018;6:e5787. doi:10.7717/peerj.5787

Supplementary material

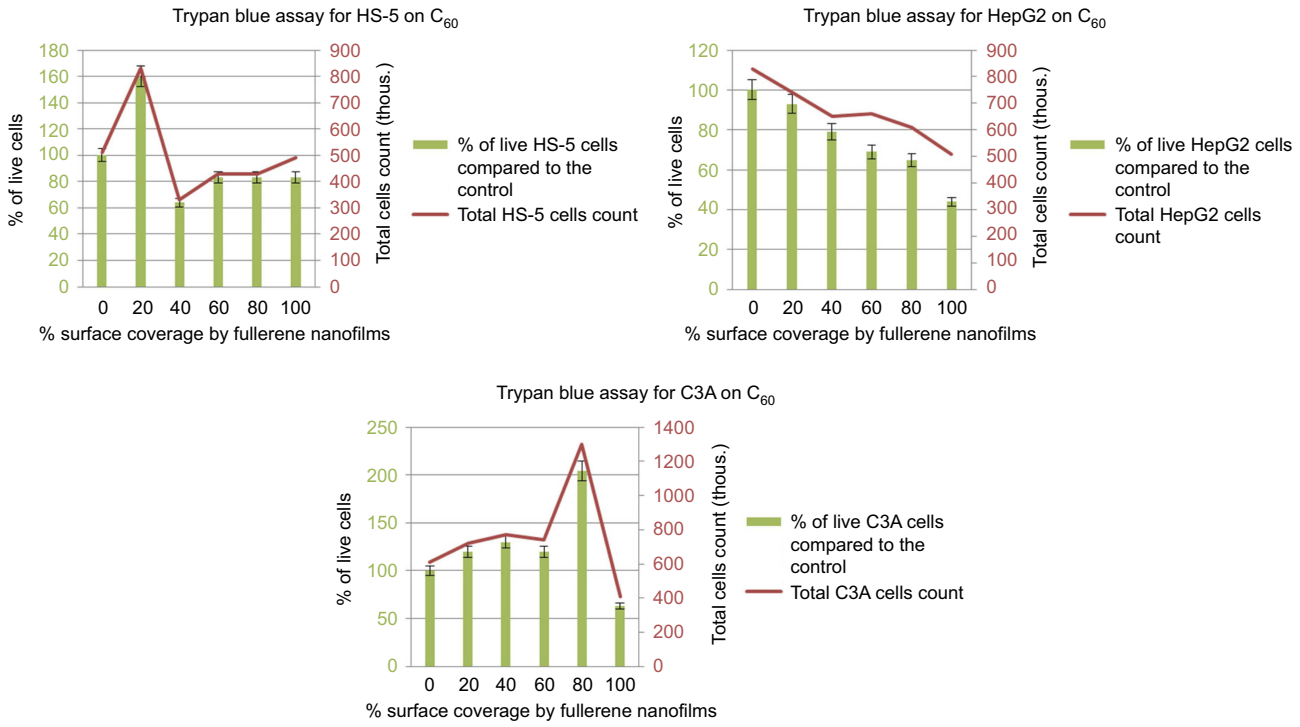

Figure S1 Results of trypan blue analysis for HS-5, HepG2 and C3A cells. Total cell count (red color) and numbers of live cells (green color) on C_{60} nanofilms.